LASER INTERFEROMETER GRAVITATIONAL WAVE OBSERVATORY
- LIGO -
CALIFORNIA INSTITUTE OF TECHNOLOGY
MASSACHUSETTS INSTITUTE OF TECHNOLOGY

Technical Note **LIGO-T2100198–v1** 2021/08/16

Back-action evasion for PT-symmetric interferometer

Student: Kagan Yanik
Mentors: Rana Adhikari, Yanbei Chen, Xiang Li, Shruti Jose Maliakal

California Institute of Technology
LIGO Project, MS 18-34
Pasadena, CA 91125
Phone (626) 395-2129
Fax (626) 304-9834
E-mail: info@ligo.caltech.edu

Massachusetts Institute of Technology
LIGO Project, Room NW22-295
Cambridge, MA 02139
Phone (617) 253-4824
Fax (617) 253-7014
E-mail: info@ligo.mit.edu

LIGO Hanford Observatory
Route 10, Mile Marker 2
Richland, WA 99352
Phone (509) 372-8106
Fax (509) 372-8137
E-mail: info@ligo.caltech.edu

LIGO Livingston Observatory
19100 LIGO Lane
Livingston, LA 70754
Phone (225) 686-3100
Fax (225) 686-7189
E-mail: info@ligo.caltech.edu

http://www.ligo.caltech.edu/

1 Introduction/Background

1.1 General Intro

Future gravitational and astrophysical research calls for the broadband and high-frequency sensitivity of gravitational wave detectors. Conventional resonant detectors are subject to bandwidth-peak sensitivity trade-off. The idea to circumvent this limitation, i.e. to improve the bandwidth without sacrificing the peak sensitivity, is called White Light Cavity (WLC). The PT-symmetric interferometer with coherent quantum feedback [1] is a stable realization of WLC (which is called sWLC for short), compared with the direct attachment of a filter cavity with anomalous dispersion [2] (uWLC for short). However, the original proposal [1] hasn't considered the back-action noise caused by the radiation pressure on the test mass.

In this project, we work with the PT symmetric interferometer. We aim to explore a more complete PT-symmetric structure to improve the low-frequency noise spectrum by back-action evasion with an effective negative mass. The effective negative mass will be possibly achieved using parametric amplification and optical damping formed by multiple additional pumpings. and hence, have a larger bandwidth with sacrificing less of the sensitivity than we would for a conventional trade-off between the bandwidth and sensitivity.

In Gravitational Wave detection, we mainly use laser interferometers, especially Michelson-type interferometers with suspended mirrors (suspended mirrors behave as free mass above the resonance frequency [7]). Gravitational waves incident on an interferometer exert a signal force on the interferometer, which causes optical displacement between the end mirrors of the interferometer. The dimensionless parameter describing the amplitude of this displacement is called strain (h) and the optical displacement (path length change) is expressed by

$$\delta x = Lh \tag{1}$$

where L is the arm length [7]. In our project, we use an arm cavity for this purpose and express it with the differential mode $\hat{a}$ since the output of the cavity depends on the differential phase between the two arms of the cavity.

1.2 Bandwidth Sensitivity Trade-off

In a setup with an arm cavity and a strain signal that comes to detector, we see a trade-off between the bandwidth and the peak sensitivity of the strain noise at the detector as a result of Energetic Quantum Limit (EQL) which is represented by the inequality [1]

$$\int_0^{+\infty} d\Omega/(2\pi) S_h^{-1}(\Omega) \leq \Delta\mathcal{E}^2/(4\hbar)^2 \tag{2}$$

If we want a larger bandwidth, we would have to have a flatter peak sensitivity and for a sharper peak sensitivity, we would have a smaller bandwidth for the strain noise being detected, hence the trade-off.

1.3 Anomalous Dispersion

To deal with the restraints of the EQL, we need to create anomalous dispersion [2]. The arm cavity from the initial setup has phase delay. We attach a filter cavity (which has a movable mirror with mechanical oscillation frequency ω_m), to the arm cavity, with phase advance to compensate for the phase delay. From the phase point of view, the two cavities can be thought as the time reversal of each other. As a result, we have a zero and constant phase for much larger bandwidth for light circulating inside the two cavities. This can be achieved by anomalous dispersion, which is a parametric interaction and helps us realize the white light cavity. Assuming that the arm cavity with the phase delay has resonant frequency ω_0, we pump the filter cavity with the detuned light at the frequency $\omega_0 + \omega_m$ [2]. As a result of this parametric interaction, we get to have a larger bandwidth, at the same level of sensitivity as before. However, this parametric interaction is unstable.

1.4 PT-symmetric Interferometer

Even though the unstable White Light Cavity (uWLC) can overcome the bandwidth sensitivity trade-off, we seek to stabilize the system, because unstability brings technical complications with the feedback control of the system. In the uWLC system,

To stabilize the system we will use a coherent quantum feedback with PT-symmetry where we place the detector at the end of the filter cavity to get the readout. It can be seen from FIG. 1 that in the unstable case (uWLC) modes $\hat{b}$ and $\hat{c}$ are at the filter cavity and attached to the arm cavity (mode $\hat{a}$) from which we get the readout. On the other hand, for sWLC, we get the readout from the filter cavity (mode $\hat{b}$) which also satisfies the PT-symmetry.

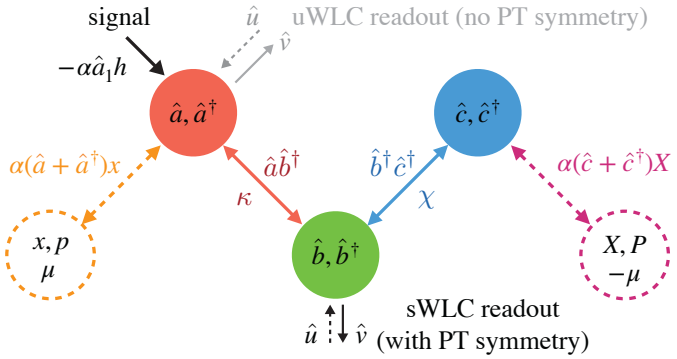

Figure 1: The stable White Light Cavity (sWLC) scheme [1]. The arm cavity has mode $\hat{a}$, the filter cavity has mode $\hat{c}$ and the detector has mode $\hat{b}$. Mode $\hat{a}$ couples to mode $\hat{b}$ with a coupling rate κ and mode $\hat{c}$ couples to mode $\hat{b}$ with coupling rate χ. Mode $\hat{b}$ is coupled to stable WLC (sWLC) readout. This system is PT symmetric when χ=κ. $\hat{u}$ is the input vacuum noise (quantum noise) and $\hat{v}$ is the output field.

Both for the uWLC and sWLC, the interaction Hamiltonian is expressed as [1]

$$\hat{V}_{\text{int}} = i\hbar\kappa(\hat{a}\hat{b}^\dagger - \hat{a}^\dagger\hat{b}) + i\hbar\chi(\hat{b}^\dagger\hat{c}^\dagger - \hat{b}\hat{c}). \tag{3}$$

1.5 Coherent Quantum Feedback

In the unstable White Light Cavity system (uWLC), discussed in the anomalous dispersion section, the filter cavity attached to the arm cavity acts as a coherent quantum feedback controller.

Looking at the equations of motion for modes, $\hat{a}$, $\hat{b}$, and $\hat{c}$ [1]

$$\dot{\hat{a}} = -\kappa\hat{b} + i\alpha h \tag{4}$$

$$\dot{\hat{c}}^{\dagger} = \chi\hat{b} \tag{5}$$

$$\dot{\hat{b}} = -\gamma_R\hat{b} + \kappa\hat{a} + \chi\hat{c}^{\dagger} + \sqrt{2\gamma_R}\hat{u} \tag{6}$$

and ignoring the signal part of mode $\hat{a}$ (iαh), we see that in the PT symmetric case, the equations of motion for mode $\hat{a}$ and $\hat{c}^{\dagger}$ are equal and opposite. Therefore, the following expression

$$\frac{d}{dt}(\chi\hat{a} + \kappa\hat{c}^{\dagger}) = i\chi\alpha h \tag{7}$$

is exclusively dependent on the signal [1]. In this equation, we obtain an internal mode (the expression inside the time derivative) which responds to the signal only, providing a coherent quantum feedback inside the system (between the modes $\hat{a}$ and $\hat{c}$). The internal mode is also a part of the readout mode ($\hat{b}$), but it is not influenced by the noise from the readout.

In this project we aim to use the coherent quantum feedback to stabilize our system.

1.6 Backaction

Gravitational waves apply a classical signal force on the movable mirror (a test mass acting as a mechanical oscillator) of the cavity and causes displacement of the mirror. Since the displacement of the mirror changes the length of the cavity, this creates very small variations in the phase of the field. Hence, the displacement can be read out from the phase of the optical field. Simultaneously, the amplitude fluctuations of the optical field provide an additional backaction force on the mirror which drives the momentum of the mirror. As a result, the position of the mirror also changes and the phase shift of the optical field due to this force indicates the backaction noise.

The backaction noise will increase when we increase the pumping power of the laser. In our project, we observe backaction when the strong field interacts with the test mass μ with mode (x,p) attached to mode $\hat{a}$. Due to backaction, both the conventional and any WLC noise spectra have a tail at low frequencies [1] where radiation pressure noise is effective, which can be seen in FIG. 2.

2 Objectives

2.1 Backaction Evasion

In this project, our objective is to add back-action evasion module to realize the full PT-symmetric structure of FIG. 1 which has not been described in prior work [1]. To preserve

the PT-symmetry structure of the system, (since $\hat{a}$ and $\hat{c}$ are PT-symmetric) we aim to attach another mode (X,P) with negative mass $-\mu$ to mode $\hat{c}$. The P-symmetry is done by attaching (X,P) to $\hat{c}$ and T-symmetry is preserved by the negative mass since $\dot{X} = \frac{P}{-\mu}$. Conserving the PT-symmetry of the system causes backaction evasion, which flattens the tails of uWLC and sWLC noise spectrum curves at low frequencies.

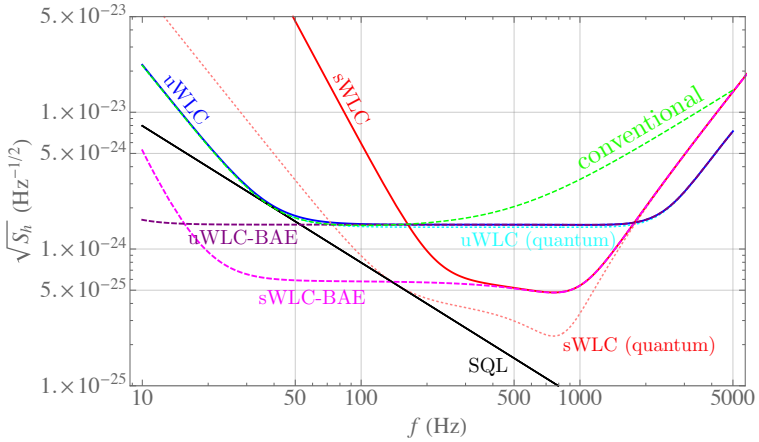

Figure 2: GW noise spectra for sWLC and uWLC both with and without backaction evasion (BAE) [1]. We can see that the tails of uWLC and sWLC at low frequencies have been flattened more due to backaction evasion.

3 Approach

3.1 Negative Mass

The complete description of the system includes the optomechanical interaction between test mass (x, p) and the cavity mode $\hat{a}$. The total Hamiltonian is given by

$$\hat{H} = \alpha(\hat{a} + \hat{a}^\dagger)x + \frac{\hat{p}^2}{2\mu} + \hat{V}_{\rm int}, \tag{8}$$

where μ is the reduced mass of the cavity mirrors, and $\hat{V}_{\rm int}$ is given in Eq. (3) where the PT-symmetry was initially constructed by adding a filter cavity to the arm cavity. Considering the interaction between mode $\hat{a}$ and the test mass (x, p), the PT-symmetry is no longer reserved. To restore the PT-symmetry of the system, we need to add a negative mass counterpart and attach it to mode $\hat{c}$:

$$\hat{V}_{\rm aux} = \alpha(\hat{c} + \hat{c}^\dagger)X + \frac{\hat{P}^2}{-2\mu}. \tag{9}$$

Attaching (X, P) to mode $\hat{c}$will conserve the P-symmetry, while the negative mass will conserve the time reversal symmetry.

To implement this negative mass in our system, we propose to add an optomechanical auxiliary mode ($\hat{d}$, $\hat{d}^\dagger$), which is expressed by the Hamiltonian

$$\hat{V}_{\rm aux} = -\hbar\alpha_d X^{\rm d}_{\rm ZPF}\hat{c}_1\hat{d}_1 - \hbar\omega_d\hat{d}^\dagger\hat{d} \tag{10}$$

with $X^{\rm d}_{\rm ZPF} = \sqrt{\hbar/(2\mu\omega_d)}$ and ω_d being the fictitious mechanical resonant frequency. $\alpha_d = \omega_{p1}/L_d$ is the dispersive coupling strength of the interaction, $\hat{c}_1$ and $\hat{c}_1$ are the amplitude quadratures of modes $\hat{c}$ and $\hat{d}$.

Besides this optomechanical system, other realizations such as a nonlinear crystal realization can potentially achieve similar results.

4 Progress

4.1 Correcting the parameters for the GW Noise Spectra for sWLC with Backaction

To obtain GW Noise Spectra in LIGO range (10 Hz - 10 kHz), we corrected the parameters being used in simulating the spectral density plots. For these parameters, we used the LIGO Voyager parameters [1]. We then compared the four cases of sWLC with the conventional detector which consists of single arm cavity with a test mass attached to it. From FIG.6, we can see that for BAE with no thermal noise, we achieve a broader bandwidth with much better sensitivity than the conventional detector.

Parameter	Value
γ_R	(2π)500 Hz
Q	8×10^9
κ	(2π)5000 Hz
χ	(2π)5000 Hz
k_B	1.38065×10^{-23} $m^2s^{-2}kgK^{-1}$
T	4 K
μ	50 kg
μc	-50 kg
ω_m	(2π)10 kHz
ω_0	$(2\pi)299792458$ $ms^{-1}/2\mu m$
$\hbar$	$1.054571628\times10^{-34}$ Js
L_{arm}	4000 m
c	299792458 ms^{-1}
P_c	3×10^6 Watt

Table 1: LIGO Voyager parameters [1] used in GW Noise Spectra.

4.2 Achieving Negative Mass Hamiltonian

In this project, we aim to cancel the backaction noise resulting from the radiation pressure force on the test mass attached to the arm cavity. To achieve BAE we aim to attach to mode $\hat{c}$ (mechanical oscillator) an auxiliary mode $(X, P) \sim (\hat{d}, \hat{d}^\dagger)$ with effective negative mass $-\mu$, in order to achieve the (effective) Hamiltonian in Eq.(10).

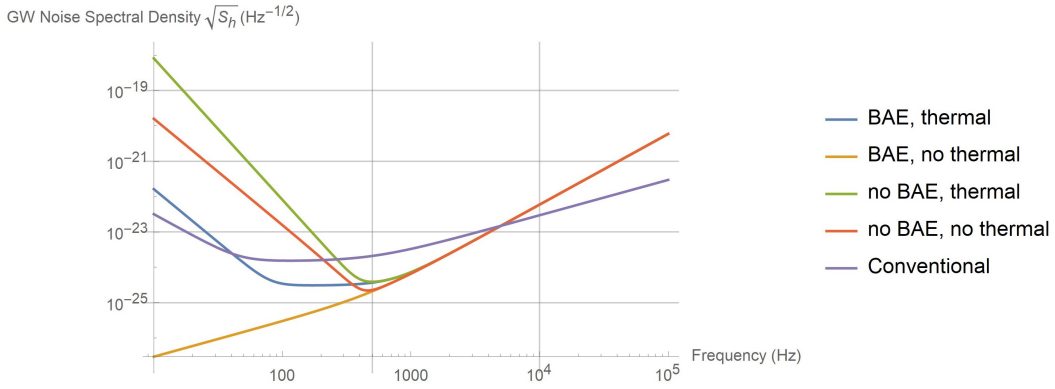

Figure 3: Normalized noise spectral density for the four cases mentioned previously for the parameters $\gamma_R = 2\pi(500)Hz, \gamma_m = 2\pi\omega_m/(2Q)Hz$ or $0Hz$ (depending on the case), $\kappa = \chi = 10\gamma_R, L = 4000m, -\mu_c = \mu = 50kg, T = 4K, \omega_m = 10kHz$, Q=8x10^9.

where α_d is proportional to the dispersive coupling constant between $\hat{c}$ and $\hat{d}$, $x_{\rm ZPF}^{\rm ETM}$ is the zero point fluctuation of the effective test mass of the mechanical oscillator. Based on the Hamiltonian we realized that we need blue and red-detuned pumping and detuning. We derived the necessary expressions to characterize the power required for both pumping and how much detuning we need from the resonant frequency of the optical mode $\hat{d}$ (ω_D).

4.2.1 PI/BS interaction

Parametric interaction and beam splitter interaction happen as a result of blue-detuned pumping and red-detuned pumping respectively. These are achieved as a result of the interaction between the mechanical oscillator $\hat{c}$ and the optical mode $\hat{d}$ of the negative mass inside filter cavity. This corresponds to the first term of the Hamiltonian in Eq.(10). In the mechanical rotating frame we express the coupling Hamiltonian between $\hat{c}$ and $\hat{d}$ as

$$\begin{aligned}\hat{V}_{\rm PI/BS} = \alpha_d x_{\rm ZPF}^{\rm c}(\hat{c}e^{-i\omega_m t} + \hat{c^\dagger}e^{i\omega_m t})(D_1 e^{-i\omega_{p1}t} + D_2 e^{-i\omega_{p2}t} + \hat{d}e^{-i\omega_D t}) \\ (D_1 e^{i\omega_{p1}t} + D_2 e^{i\omega_{p2}t} + \hat{d^\dagger}e^{i\omega_D t}).\end{aligned} \tag{11}$$

The frequency match condition for blue and red-detuned pumping are $\omega_{p1} = \omega_D + \omega_m$ and $\omega_{p2} = \omega_D - \omega_m$ respectively. Applying these conditions to Eq.(11), we get

$$\hat{V}_{\rm PI/BS} = \alpha_d x_{\rm ZPF}^{\rm c}(D_1(\hat{c}\hat{d} + \hat{c^\dagger}\hat{d^\dagger}) + D_2(\hat{c^\dagger}\hat{d} + \hat{c}\hat{d^\dagger})). \tag{12}$$

Since we aim to cancel the backaction in the Hamiltonian, we need to satisfy the following relation:

$$\alpha_d x_{\rm ZPF}^{\rm c} D_1 = \alpha x_{\rm ZPF}^{\rm ETM} \tag{13}$$

where $\alpha = \sqrt{2P_c\hbar\omega_0/L_a c}$ and $x_{\rm ZPF}^{\rm ETM} = \sqrt{\hbar/2\mu\omega_m^{\rm ETM}}$. Taking D_1 as the cavity mode amplitude, we get the following expression for the relation

$$\frac{\hbar\omega_{p1}}{L_d}\sqrt{\frac{\hbar}{2m_c\omega_m}}\sqrt{\frac{P_1 L_d}{2\pi\hbar\omega_{p1}c}} = \alpha X_{\rm ZPF}^{\rm d} \tag{14}$$

where m_c and ω_m are the mass and angular frequency of the oscillator respectively, P_1 and $\omega_{p1} = \omega_D + \omega_m$ are the power and angular frequency of blue-detuned pumping respectively. We took $\alpha_d = \hbar\omega_{p1}/L_d$ where ω_{p1}/L_d is the dispersive coupling strength of the interaction. From Eq.(14), we can derive the expression to characterize the pumping power to achieve blue-detuned pumping:

$$P1 = 4\pi\left(\frac{L_d}{L_a}\right)\left(\frac{m_c}{\mu}\right)\left(\frac{\omega_m}{\omega_d}\right)\left(\frac{\omega_0}{\omega_{p1}}\right)P_c \tag{15}$$

where P_c is the power at the arm cavity and L_a is the arm cavity length. Same expression can be found for the red-detuned pumping by changing P_1 to P_2 and ω_{p1} to ω_{p2}.

4.2.2 Detuning

Another pumping is done at an angular frequency (ω_{p0}) near the resonant frequency (ω_d) of $\hat{d}$ which is detuned by angular frequency Δ ($\omega_{p0} = \omega_d + \Delta$). This is achieved by the terms $\hat{d}\hat{d}^\dagger$ and $\hat{d}^\dagger\hat{d}$ which are present in the momentum operator of the Hamiltonian in Eq.(**??**). Hence, for detuning, we get the following Hamiltonian

$$\hat{V}_{\rm det} = \hbar\frac{\hbar}{8\mu(x_{\rm ZPF}^{\rm ETM})^2}(-\hat{d}\hat{d}^\dagger - \hat{d}^\dagger\hat{d}). \tag{16}$$

Using the conjugate pair relation $[\hat{d}, \hat{d}^\dagger]$=1, we simplify the Hamiltonian to

$$\hat{V}_{\rm det} = \hbar\frac{\hbar}{-4\mu(x_{\rm ZPF}^{\rm ETM})^2}(\hat{d}^\dagger\hat{d} + \frac{1}{2}). \tag{17}$$

Ignoring the vacuum component of the Hamiltonian we can express its coefficient by equating the Hamiltonian to the detuning component of the quantum harmonic oscillator Hamiltonian $\hbar\Delta\hat{d}^\dagger\hat{d}$. Hence, we get the relation

$$\Delta = \frac{\hbar}{-4\mu(x_{\rm ZPF}^{\rm ETM})^2}. \tag{18}$$

For $x_{\rm ZPF}^{\rm ETM} = \sqrt{\frac{\hbar}{2\mu\omega_m^{\rm ETM}}}$, we get the relation

$$\Delta = -\frac{\omega_m^{\rm ETM}}{2}, \tag{19}$$

where $\omega_m^{\rm ETM} \approx 1$Hz is the resonant frequency of arm cavity test mass. The $\hbar\Delta$ just reveals the nature of "negative mass" zero point fluctuation.

4.3 Simulating the system in FINESSE

We have worked on FINESSE to simulate the filter cavity (mode $\hat{b}$) and show the anomalous dispersion. While most of the FINESSE code is completed towards simulating the cavity, there are some parameters and issues that remain to be fixed.

We started with the basics of the filter cavity by simulating a simple Fabry-Perot (FP) cavity with a fixed input mirror and a movable end mirror and applied a blue-detuned laser. For the FP cavity, we have shown the resonance condition works by looking at the circulating, reflected and transmitted power at varying detuning of the input mirror since we get peak transmitted and circulating power and minimum reflected power at every 180 degree detuning.

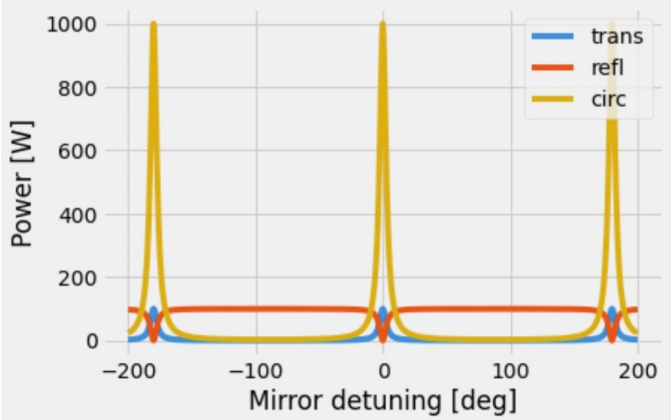

Figure 4: Circulating, reflected and transmitted power for varying detuning of the input mirror. Laser power is 100 W, cavity length is 4m.

We then checked the FP cavity without laser detuning to check the mechanics of the FP cavity by applying a mechanical transfer function to both mirrors. In this case, we only see a single peak in the displacement of both mirrors, which shows the mechanical resonance frequency.

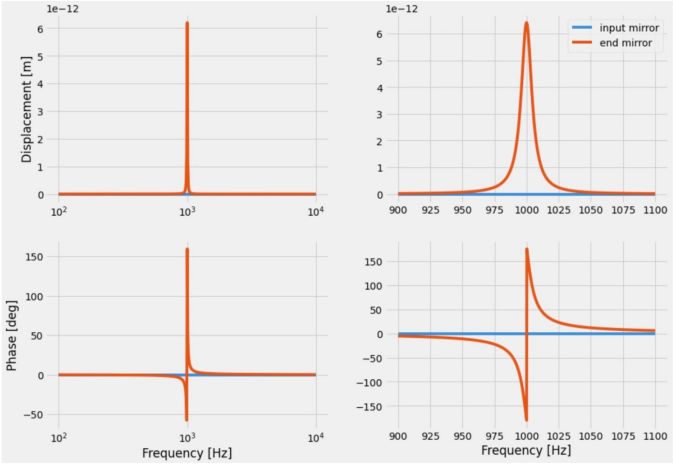

Figure 5: Displacement of mirrors vs signal force frequency in logarithmic scale (upper left) and linear scale (upper right). Relative phase to the force signal for both mirrors in logarithmic (lower left) and linear scale (lower right). Cavity is not detuned.

Then we checked the mechanical response of the oscillator for blue-detuned pumping to see

the optical spring effect causing a shift in mechanical resonance frequency.

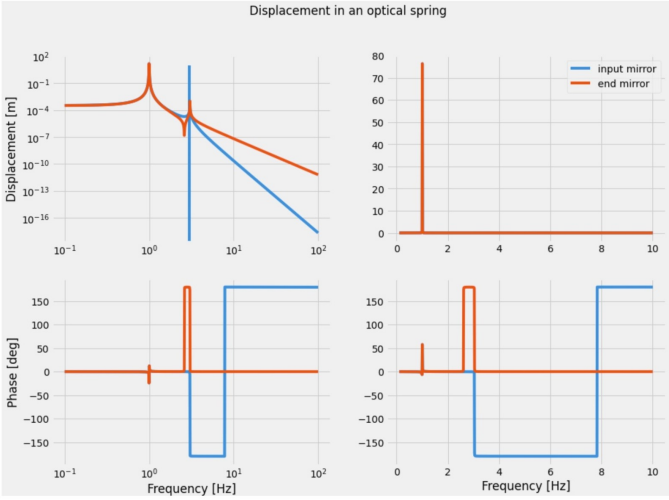

Figure 6: Displacement of mirrors vs signal force frequency in logarithmic scale (upper left) and linear scale (upper right). Relative phase to the force signal for both mirrors in logarithmic (lower left) and linear scale (lower right). Cavity is detuned.

5 Future Directions

For the next steps of our project, we aim to correct the problems with the FINESSE code to simulate the filter cavity, show the anomalous dispersion phase plots, input-output relations and compare them with the expected results. After that, we will be coupling the arm cavity to the filter cavity in FINESSE. We will also be evaluating how losses in any given mirrors of the armand filter cavity and how they affect the input-output relations and noise spectrum.

For the effective negative mass, by using the right parameters, we will be calculating the power necessary for each pumping and detuning to realize the effective negative mass, design figure of merit and numerically optimize for the Hamiltonian we have for the negative mass. We will also be simulating the negative mass in Finesse.

References

[1] Li, Xiang, et al, *Broadband sensitivity improvement via coherent quantum feedback with PT symmetry*. arXiv preprint arXiv:2012.00836 (2020).

[2] Miao, Haixing, et al, *Enhancing the Bandwidth of Gravitational-Wave Detectors with Unstable Optomechanical Filters*. Phys. Rev. Lett. 115, 211104

[3] Chen, Yanbei, *Macroscopic quantum mechanics: theory and experimental concepts of optomechanics*. Journal of Physics B: Atomic, Molecular and Optical Physics 46.10 (2013): 104001.

[4] Li, Xiang, et al, *Supplementary Material for Broadband sensitivity improvement via coherent quantum feedback with PT symmetry.*

[5] Tsang, Mankei and Caves, Carlton M. *Evading quantum mechanics.* arXiv preprint arXiv:1203.2317 (2012).

[6] Khalili, F. Ya. and Polzik, E. S. *Overcoming the Standard Quantum Limit in Gravitational Wave Detectors Using Spin Systems with a Negative Effective Mass.* Phys. Rev. Lett. 121, 031101

[7] Arai, Koji, *Gravitational wave detection with laser interferometers.* LIGO SURF 2021 Lecture Presentation.

[8] Adhikari, Rana X., et al, *A Cryogenic Silicon Interferometer for Gravitational-wave Detection.* Classical and Quantum Gravity 37, no. 16 (2020): 165003.